Chemical Engineering Journal 475 (2023) 146278

Contents lists available at ScienceDirect

Chemical Engineering Journal

journal homepage: www.elsevier.com/locate/cej

ATP-responsive and functionalized framework nucleic acid for synergistic radio-immunotherapy

Yuxin Zhang [a], Yuxi Zhan [a], Chenchen Mao [a], Guo Li [a], Yuxuan Zhao [a], Ye Chen [a], Yunfeng Lin [a,b,*]

[a] State Key Laboratory of Oral Diseases, National Center for Stomatology, National Clinical Research Center for Oral Diseases, West China Hospital of Stomatology, Sichuan University, Chengdu 610041, China
[b] Sichuan Provincial Engineering Research Center of Oral Biomaterials, Chengdu, Sichuan 610041, China

ARTICLE INFO

Keywords:
Tetrahedral framework nucleic acid structure
Immunoadjuvant-functionalized nanostructure
ATP-responsive nanostructure
Radio-immunotherapy

ABSTRACT

Traditional radiotherapy is ineffective against some aggressive and recurrent tumors. In clinical therapy, low-dose radiations are frequently utilized to lessen the negative effects of X-rays. There is an urgent need to develop a novel therapeutic strategy for adjuvant radiotherapy. An ATP-responsive and functionalized framework nucleic acid delivery system (Op-TGA) was developed using local irradiation, which can cause enormous ATP release from tumors. The framework nucleic acid carrying the nucleic acid fragment of immune adjuvant and antigen peptides can be massively aggregated and successfully released in a high-concentration ATP environment using this delivery platform. Thus, intravenous injection of Op-TGA into tumor-bearing mice after radiation can precisely concentrate around the tumor tissue, and once released, it is rapidly taken up by antigen-presenting cells, stimulating the cellular immune response. The conjunction of radiotherapy and Op-TGA has a significant synergistic anticancer efficacy and establishes an immunological memory effect to prevent tumor recurrence. Op-TGA developed here offers a new technique for Radio-immunotherapy that is closely related to clinical therapy and has great clinical application potential.

1. Introduction

Radiotherapy (RT) is a prevalent cancer treatment approach that has been widely used to treat most localized solid tumors at various stages. After RT, the tumor may undergo immunogenic cell death (ICD) [1]. During the ICD in tumors, several signaling molecules, known as damage-related molecular patterns (DAMPs), are produced [2]. These signaling molecules include calreticulin (CRT) on the cell surface, high mobility group protein 1 (HMGB 1) secreted by tumor cells to the outside world, ATP molecules released by cells, and heat shock proteins (HSP70, HSP90), etc. [3,4]. DAMPs generated during ICD can bind to pattern recognition receptors (PRRs) on the surface of dendritic cells (DCs) to trigger a cascade of biological reactions, which ultimately activate innate and adaptive immune responses [5]. In contrast, the anti-tumor immune response induced by RT is insufficient in clinical settings. Thus, it is anticipated that enhancing the immune response caused by RT can enhance the antitumor impact without increasing the RT dosage. Scheme 1

Immunoadjuvants are supplementary stimulants that improve or modify the immune response to an antigen by accelerating antigen processing and boosting the effectiveness of antigen-presenting cells (APC) [6,7]. When tumor cells are treated with radiation, a number of antigens are released rapidly. These antigens are delivered to T lymphocytes by APC. T lymphocytes create lymphokines and target primary and metastatic tumor cells. Therefore, the incorporation of immune adjuvants into the ICD procedure can result in the enhancement of anti-tumor immune responses [8,9]. However, the majority of presently used immunoadjuvants are inorganic adjuvants or compounds with a certain level of biological toxicity, which lack targeting in general [10–12]. Off-target effects generated by these components might result in severe adverse effects, such as cytokine storm or autoimmune illnesses, hence limiting its therapeutic applicability [13]. New nano-adjuvants are appearing as a result of the ongoing advancements in nanotechnology, offering a fresh approach to successfully resolving the aforementioned problems [12,14]. Based on these challenges, we developed an ATP-Responsive and immunoadjuvant-functionalized framework nucleic

* Corresponding author at: State Key Laboratory of Oral Diseases, National Center for Stomatology, National Clinical Research Center for Oral Diseases, West China Hospital of Stomatology, Sichuan University, Chengdu 610041, China.
E-mail address: yunfenglin@scu.edu.cn (Y. Lin).

https://doi.org/10.1016/j.cej.2023.146278
Received 27 May 2023; Received in revised form 16 August 2023; Accepted 24 September 2023
Available online 25 September 2023

acid for the exact delivery and release of antigens and adjuvants to immune cells near tumor foci.

In our developed nanostructure of tetrahedral framework nucleic acid (tFNA), a single-stranded DNA CpG oligonucleotide with an extended strand complementary to an ATP aptamer is loaded (TG). The ATP aptamer then binds to the expanded strand through complementary base pairing (TGA). And the OVA antigen peptide (SIINFEKL) was chemically linked to another vertex of tFNA (Op-TGA). Following local RT of tumor lesions, the ICD of tumor cells promotes the release of significant quantities of ATP from tumor cells. There are high concentrations of ATP in the tumor microenvironment (TME) [14–16]. ATP aptamers undergo allosteric under ATP competition to ensure the targeted and controlled release of Op-TG when a significant quantity of ATP is generated. Op-TG is taken up by APCs surrounding tumor lesions, triggering a robust antitumor immune response to augment RT synergistically. The efficacy of the nanostructures was evaluated by using mouse melanoma B16-F10 and OVA-B16-F10 tumor models. Melanoma growth was reduced dramatically and significantly better than with RT alone. After a period of therapy, mice generated a substantial number of immunological memory cells. Herein, Antigen peptide and Immunoadjuvant were loaded onto tetrahedral DNA nanostructures for the first time, and it may be collected in vast amounts surrounding tumor tissue with a high concentration of ATP to provide precisely directed release. Thus, the creation of ATP-responsive and immunoadjuvant-functionalized framework nucleic acid for radio-immunotherapy synergy would be a therapeutically significant technique.

2. Material and methods

2.1. Materials

B16 and OVA-B16 cell lines were obtained from the American Tissue Type Collection (ATCC). C57BL/6 mice were purchased from Beijng HFK BIOSCIENCE Co. Ltd. (Beijing, China). Single-stranded DNAs (ssDNAs) with specific sequences were obtained from TaKaRa (Dalian, China). ssDNA sequences were listed in Table S1. OVA peptide was obtained from Sangon Biotech (Shanghai, China). ELISA kits were purchased from Universal Biotech (Shanghai) or RUIXIN BIOTECH (Quanzhou). ATP assay kit was purchased from Beyotime (Shanghai, China). All primary antibodies purchased from CST (MA, USA) or Abcam

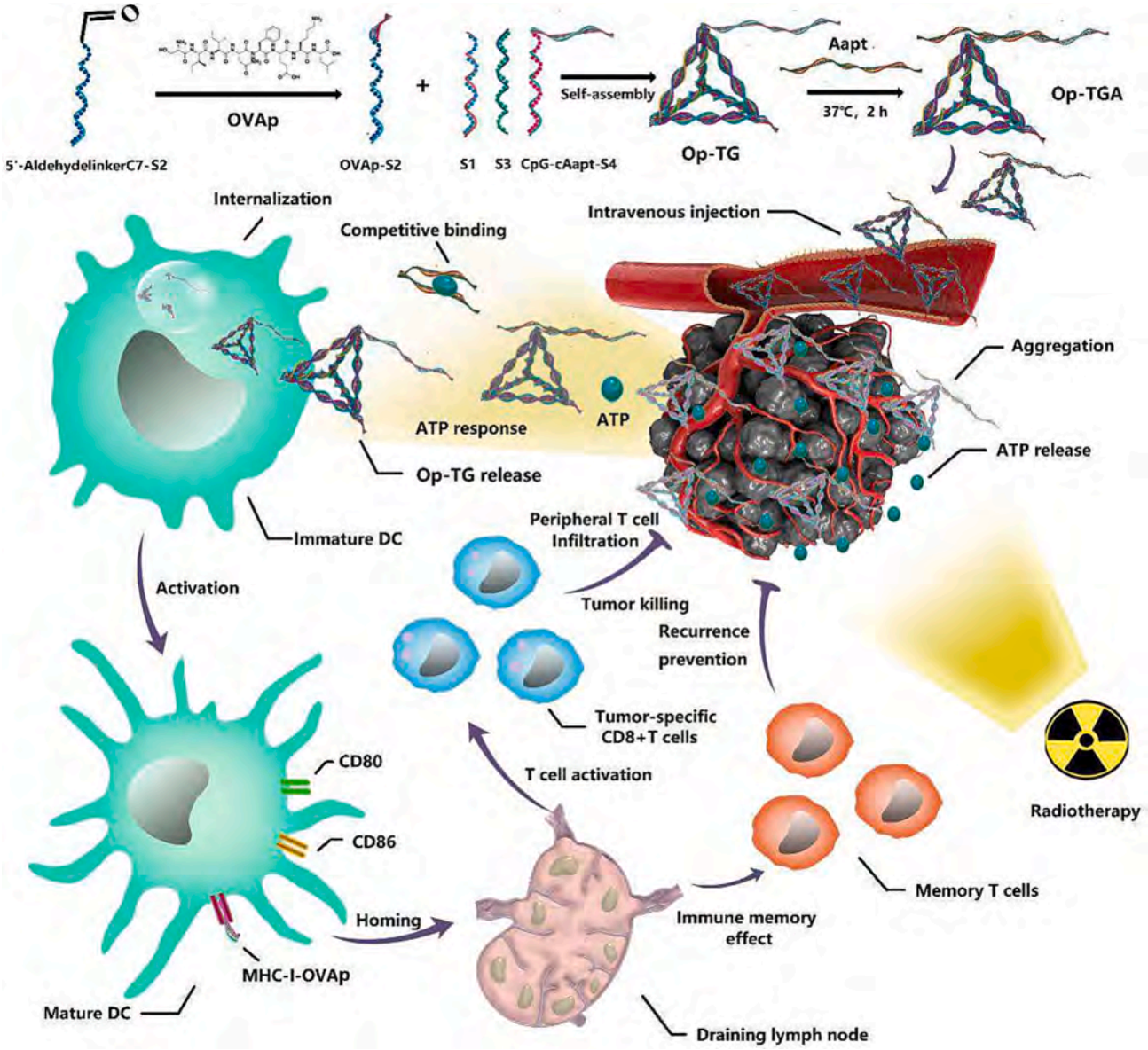

Scheme 1. Schematic illustration showing Op-TGA formation and mode of action.

were used in Immunohistochemistry or immunofluorescence and listed in Table S2. The flow cytometry antibodies were obtained from Biolegend and listed in Table S2.

2.2. Ligation of OVA peptide to ssDNA and characterization

In our earlier study, tFNA was comprised of four ssDNAs (called S1-S4). In this study, the S2 was pre-modified with 5′-AldehydelinkerC7 as a connecting site for chemical linkage with the OVA peptide. It subsequently experiences a condensation reaction with the amino group on the OVA peptide, and then the crude compound OVAp-S2 is obtained, and the product is purified by HPLC [17]. After the eluate was filtered with a 30 kDa filter, mass spectrometry was utilized to determine if its molecular weight corresponded to the desired product.

2.3. Self-Assembly and characterization of ATP-Responsive and functionalized framework nucleic acids

According to the previously reported approach, CpG-cAapt is linked to S4 (CpG-cAapt-S4) and self-assembles with S1, OVAp-S2, and S3 to produce Op-TG. The TG comprises S1, S2, CpG-cAapt-S4, and S3 [18–22]. After incubating Op-TG with Aapt (Op-TG/Aapt ratio: 1:2) for 2 h at 20℃, the mixture was filtered through a 30 kDa membrane to remove unbound Aapt. To verify the successful binding of Aapt to Op-TG, Aapt carrying a fluorescence quenching group (BHQ 3) was incubated with CY5.5-Op-TG, and the system's fluorescence intensity was evaluated at various time points using a chemiluminescence analyzer (Varioskan LUX, Thermo Scientific). To validate the effective synthesis of Op-TGA, PAGE was utilized. In addition, its components were evaluated after 90 min of constant voltage operation(80 V) [23–26]. Gel-red staining to observe the mobility of each component. To investigate the morphological and dimensional features of Op-TGA, samples were placed on copper grids and observed using TEM (HT7700, Hitachi, Japan) [26]. Then lay the sample on the mica sheet for further observation with AFM (SPM-9700 instrument, Shimadzu, Kyoto, Japan) [27]. The particle sizes of tFNA, Op-tFNA, Op-TG and Op-TGA and zeta potential of Op-tFNA, Op-TG and Op-TGA were determined.

2.4. Op-TG release in response to ATP from Op-TGA

To determine whether Op-TG could be released from Op-TGA in reaction to ATP, a certain concentration of ATP was introduced to CY5.5-Op-TGA, and the fluorescence intensity of the mixture was measured every hour [28]. In parallel, the mixture incubated with ATP was examined by PAGE and Fluorescence Resonance Energy transfer (FRET) to verify that Op-TGA was successfully released, the group without ATP as a control.

2.5. In vivo and in vitro ATP measurement after RT

To determine whether the ATP concentrations in the tumor increased as a result of X-ray irradiation, we locally administered a specific dosage of X-ray radiation dose to B16-F10 tumor-bearing mice. After 16 h, luciferase and luciferin were combined in the ATP assay kit to create the detected working solution, which was subsequently injected intratumorally into tumors. 2 min later, a in vivo scanning instrument (IVIS® Spectrum) was utilized to image the tumor [29]. And ATP levels in the liver, heart, and tumor tissues were detected using an ATP assay kit. Simultaneously, B16 cells were planted on Petri plates and exposed to a variety of X-ray radiation dosages. After 16 h, the ATP concentration in the supernatant was tested.

2.6. In vivo distribution imaging of Op-TGA and Op-TG

Intravenous injections of 100 μL of CY5-Op-TGA and Op-TG (1 μM) were administered to B16-F10-bearing mouse models after RT. Mice were sedated with isoflurane at various times (1 h, 4 h) and scanned using an in vivo scanning system (IVIS® Spectrum) [29]. After photographing the living animals at each time point, the mice were killed, and their primary organs and tumor were swiftly removed in order to observe the fluorescence of isolated organs in C57BL/6 mice.

2.7. Analysis of hemolytic properties of Op-TGA and its components

To calculate the hemolysis coefficient, the content of total blood hemoglobin and free hemoglobin released into plasma after blood exposure to Op-TGA and its components was determined using quantitative colorimetry.

2.8. Assays of in vitro BMDC maturation and antigen Presentation, internalization of cells

The femur and tibia of C57BL/6 mice were used to collect bone marrow, which was then put into culture plates at a density of 2×10^6 viable cells per well. Use RPMI1640 complete medium with 20 ng/mL GM-CSF and 10 ng/mL IL-4 and grow the cells in an incubator at 37 °C with 5 % CO2. On the 1st day, the medium was changed, and then every two days, two-thirds of the medium was changed [15]. Each time the medium was changed, cytokines were added. Immature Bone Marrow-derived Dendritic Cells (BMDCs) are the non-adherent and loosely adherent cells found in the culture supernatant on the 7th day. To evaluate cellular internalization, CY5-OVA peptide (OVAp), CY5-Op-SG, and Op-TG were separately incubated with BMDCs on cell culture plates at 37 °C for 12 h, followed by CLSM evaluation. To examine the maturation stage of BMDCs, BMDCs were cultured with PBS, OVAp (1 μM), and Op-TG (500 nM) for 24 h in 6-well plates, and then harvested and stained with anti-mouse-CD45-APC/CY7, anti-mouse-CD11c-APC, anti-mouse-CD80-PE, and anti-mouse-CD86 -BV421. In order to observe the internalization of Op-TG and Op-SG by BMDCs for antigen presentation, the cells were harvested and fixed after 12 h of incubation with Op-TG and Op-SG, and ultrathin slices of DCs were prepared. OVAp was localized using anti-OVA primary antibody and 10 nm colloidal gold secondary antibody and observed by TEM. To evaluate antigen presentation, BMDCs were treated with Op-TG or Op-SG for 36 h, and then anti-mouse-H-2 Kb-FITC was utilized to bind MHC-I-OVAp, which was observed by CLSM. Flow cytometry was used to assess cells in the Op-TG group that had been treated with anti-mouse-CD45-APC/CY7, anti-mouse-CD11c-PE/CY7, and anti-mouse-H-2 Kb-APC. To demonstrate that Op-TG-treated DCs can stimulate the proliferation of lymphocytes, mouse spleen lymphocytes were isolated using a spleen lymphocyte isolation kit. Different ratios of Op-TG-treated DCs were co-cultured with spleen lymphocytes, and the proliferation rate of lymphocytes was determined using CCK-8.

2.9. Cytokine analysis

The supernatants of BMDCs from C57BL/6 mice incubated with OVAp, Op-SG, or Op-TG for 24 h were harvested. And ELISA kits are utilized to evaluate TNFα, IFNγ, IL-1β, and IL-12p70 [30]. Tumor tissue homogenates and serum from tumor-bearing mice were collected to evaluate TNF-α, IFN-γ by ELISA kits.

2.10. Synergistic treatment of B16-F10 or OVA-B16-F10 tumors with ATP-Responsive and immune adjuvant functionalized tFNAs and radiotherapy

B16-F10 or OVA-B16-F10 melanoma cells (1×10^6) were implanted subcutaneously on the back of C57BL/6 mice. On the 7th day after tumor implantation, therapy studies were done. On the 1st, 4th, 7th, and 10th days, tumors were given 3 Gray X-rays locally. The samples were injected into the tail vein of each mouse after 16 h of each RT. Simultaneously, tumor volumes and body weights of mice were evaluated.

The control treatment groups received the same amount of TGA, SGA, OVAp, Op-TGA, and OVAp + TGA as the experimental group described above. Mice were sacrificed on the 20th day, tumors were obtained for H&E, and TUNEL staining. The expression of CD31 in the tumor tissue was observed. RT + Op-TGA group mice had OVA-B16 re-implanted on the opposite side of their backs on 15th days, while naive mice served as controls. Observe the development of tumors in mice for 20 days.

2.11. Flow cytometry assay

Tumor tissues, lymph nodes, and spleen were transformed into single-cell suspensions following therapy. Using Percoll density gdradient centrifugation to separate lymphocytes from tumor tissue. After staining, lymphocytes were quantitatively analyzed by an Attune NxT Acoustic Focusing Cytometer (Thermo Fisher Scientific). Basically, obtained tissues were mashed with 3 mL of PBS in 6-well plates. Washing the suspension with staining buffer. Collecting cells, resuspending them in 100 μL of staining buffer, and staining them with fluorescence-conjugated antibodies. Dendritic cells (DCs) from lymph nodes were stained with anti-mouse-CD45, anti-mouse-CD11C, anti-mouse-CD80, and anti-mouse-CD86 antibodies. CD8 + T cells in tumor tissues and Spleen were tagged by anti-mouse-CD3 and anti-mouse-CD8 antibodies. Tem cells in peripheral blood were stained with anti-mouse-CD3, anti-mouse-CD8 anti-mouse-CD44, and anti-mouse-CD62L antibodies. Lymphocytes from the spleen were mixed with anti-mouse-CD3, anti-mouse-CD8, anti-mouse-CD44, and anti-mouse-CD62L antibodies. The flow cytometry antibodies were documented in Table S2.

2.12. Immunohistochemistry or immunofluorescence analyses

We used 4 % paraformaldehyde and paraffin slices to preserve the major organs and tumors of mice. Pathological examination with H&E staining. Organ and tumor paraffin slices were deparaffinized and rehydrated. Then blocked with goat serum after antigen retrieval with 10 mM citrate buffer (pH 6.0) at 95 °C for 15 min. The appropriate primary antibody is then utilized for incubation, followed by the corresponding secondary antibody [31]. Observation of images was conducted using an upright microscope (BX53, Olympus).

2.13. Statistical and data analyses

GraphPad Prism 7.0 was utilized for graph construction and turkey analysis of statistical significance. Flow cytometric studies were performed using FlowJo V10. The data are displayed as the mean ± SD. A minimum of six independent trials were conducted for each component.

3. Results

3.1. Synthesis and characterization of ATP-Responsive and Immunoadjuvant-Functionalized framework nucleic acids

The self-assembly of four single-stranded DNAs (ssDNAs) produces tetrahedral framework nucleic acids. In the current technique, the second ssDNA was pre-modified with 5′-AldehydelinkerC7 as a connecting site for chemical linkage with the OVA peptide (**FIG. 1A**), as shown by HPLC and MS analysis (**FIG. 1B, 1C**). An CpG oligonucleotide with an extended strand complementary to the ATP aptamer (CpG-cAapt) was covalently linked to 5′ of the fourth ssDNA (S4), and the effective loading of this ligation was confirmed by polyacrylamide gel electrophoresis (PAGE). The results reveal that CpG-cAapt-S4 (SG) exhibited pronounced hysteresis relative to pure S4, demonstrating that CpG-cAapt was effectively linked to S4. The pre-modified S2, S4 combined with the other ssDNAs to generate Op-TG, which was then incubated with Aapt to form Op-TGA. (**FIG. 1D**). By comparing the migration rates of tFNA, Op-TG, and Op-TGA on the PAGE, it was determined that CpG-cAapt and Aapt were successfully loaded onto tFNA (**FIG. 1E**). Using transmission electron microscopy (TEM) and atomic force microscopy (AFM) to investigate the morphology of Op-TGA, as seen in **FIG. 1F, 1G, a** tetrahedral framework structure with extended arm chains can be detected, further demonstrating the effective synthesis of Op-TGA (Fig. 1**D**). Dynamic light scattering (DLS) was then used to verify the sizes and zeta potentials of the tFNA, Op-tFNA, Op-TG and Op-TGA. Dynamic light scattering was then used to verify the sizes of the asPNA and P-TDNs. As shown in **FIG S1,S2 (Supporting Information)**, in the control groups, the average size of tFNA was 6.86 nm, the average size of Op-tFNA was 7.65 nm. However, the average size of Op-TG and Op-TGA were significantly larger than the control groups, indicating the formation of framework structures.

Furthermore, we established that Aapt and CpG-cAapt can effectively generate duplexes using the fluorophore Cy 5.5 and the quencher BHQ 3. When Aapt was double-stranded with CpG-cAapt, the quencher BHQ 3 approached the fluorophore Cy 5.5 to quench its fluorescence [32]. As shown in Fig. 2**A**, when BHQ 3-Aapt was added to Cy 5.5-Op-TG, the system's fluorescence intensity reduced with time, confirming that Aapt could bind to Op-TGA. Subsequently, we demonstrated that the duplex formed by Aapt and CpG-cAapt can be opened in response to ATP (Fig. 2**B**). As shown in Fig. 2**C**, Op-TG is released when we add varying amounts of ATP to Op-TGA and observed the dissociation of Aapt and Op-TG via the PAGE. The result indicated that Op-TG was successfully released in high ATP concentration. This structure was shown to be more suited for low-dose radiation as ATP concentration increased to a particular range. When the concentration of ATP is too high, it may mismatch with tFNA skeleton, resulting in hybrid bands. The size of Op-TGA was observed after the addition of ATP, and no significant changes were observed, indicating that the framework structure of Op-TG did not change after the dissociation of the ATP aptamer, which is more favorable for the subsequent application **(FIG S3, Supporting Information).** Subsequently, it was analyzed when Op-TGA initiates the ATP response while dissociating BHQ 3-Aapt from CY5.5-Op-TG (Fig. 2**D**). The process of switching on the ATP response is rapid. When ATP was added to Op-TGA, the fluorescence intensity of CY5.5 increased rapidly and tended to equilibrate after 10 min. Simultaneously, The fluorescence intensity of the control without ATP did not change significantly.

3.2. Effects of radiotherapy on ATP concentration in TME and assessment of the biosafety of Op-TGA

To verify that Op-TGA can respond in the proximity of tumor tissue, we assessed the radiation-induced changes in ATP concentration in tumor cells (Fig. 2**E**). With increasing RT dosage, the concentration of ATP in the medium of tumor cells increased gradually, hence facilitating the response of TGA in tumor tissue. Then, the ATP concentration in tumor tissue was measured after RT. To use in vivo imaging of small animals, the changes in ATP concentration near tumor tissue in mice before and after RT were detected. As seen in Fig. 2**F**, the ATP concentration surrounding the tumor tissue increased significantly after RT. Since luciferase cannot enter the cells, we found that the chemiluminescence signal at the tumor lesions of X-ray irradiated mice was significantly enhanced by observing the extracellular ATP content in the microenvironment of tumor tissues, which indicates that radiotherapy can lead to a significant increase in the ATP concentration in tumor tissues, which can be a prerequisite for Op-TGA to be able to assist in tumor radiotherapy. The ATP levels in liver, heart and tumor tissues in a mouse model after radiotherapy were compared and found that ATP levels in tumor tissues were much higher than those in liver and heart **(FIG. S4, Supporting Information)**. Since liver and heart are the two tissues with the highest ATP levels, this evidence further suggests that tumor tissues after radiotherapy are able to aggregate Op-TGA with ATP-responsive structures.

Moreover, we investigated whether Op-TGA could accumulate around tumor tissue after RT to complete the ATP response, and we

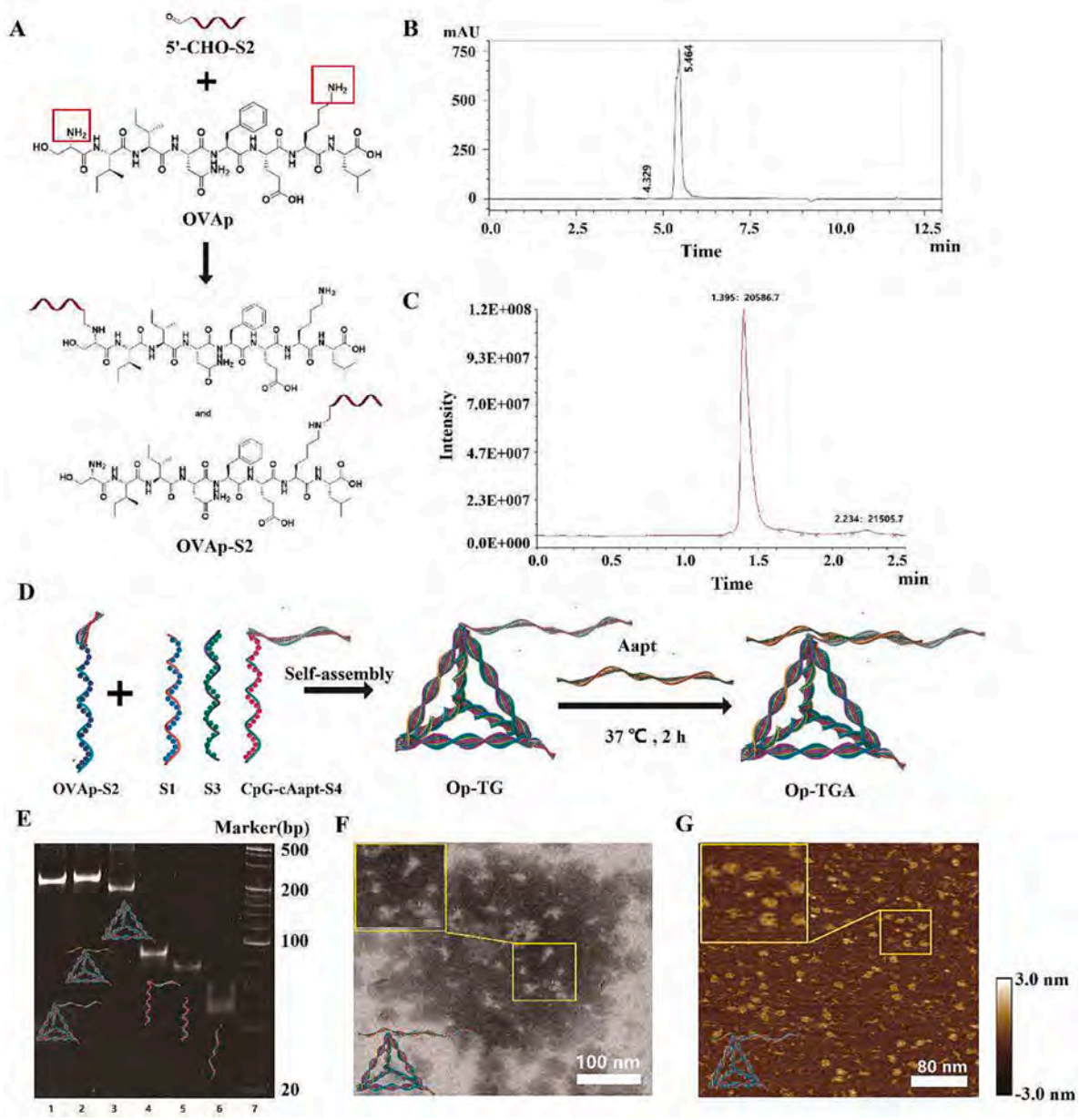

Fig. 1. Construction of ATP-Responsive and immunoadjuvant-functionalized framework nucleic acids. (A). OVAp-S2 generation schematic. (B). The HPLC results of OVAp-S2. (C). Mass Spectrometry Analysis of OVAp-S2. (D). Schematic of synthesis. (E). PAGE analysis of Op-TGA. (F). the morphology of Op-TGA graphed by TEM. (G). AFM image of Op-TGA.

observed the distribution of Op-TG and Op-TGA in mice bearing B16 tumors. Op-TG and Op-TGA was injected into mice after RT and then used in vivo imaging of small animals to observe the distribution of Op-TG and Op-TGA in tumor tissues and organs at various time periods (Fig. 2**G, 2H**). Due to the absence of ATP aptamer, Op-TG was unable to be kept in an environment with a high concentration of ATP. After radiotherapy, Op-TGA could be kept surrounding the tumor tissue, allowing time for APCs uptake. After RT, Op-TGA accumulated but Op-TG did not, surrounding the tumor tissue, indicating that the increased ATP concentration in the tissue can certainly trigger Op-TGA to accumulate in ATP response. All intravenous medications must be evaluated for their hemolytic potential; hence we examined Op-TGA and its constituents for hemolytic activity. The results indicate that Op-TGA and its constituents have extremely little hemolysis, demonstrating the system's high level of biosafety (Fig. 2**H**).

3.3. Op-TG stimulates BMDCs maturation in vitro.

We demonstrated that Op-TGA can effectively release Op-TG in response to ATP. We questioned whether Op-TG might well be taken up by APCs to activate the immune system. Since DCs are the most efficient APCs, we investigated whether the Op-TG might induce an effective immune response by stimulating bone marrow-derived DCs (BMDCs) in vitro (Fig. 3**A**). First, we used a confocal laser scanning microscope (CLSM) to confirm that Op-TG can be successfully taken up by BMDCs, the uptake efficiency of Op-TG is much greater than that of pure OVAp and SG loaded OVAp antigenic peptide (Op-SG) (**FIG. S5, Supporting Information**). Immunoelectron microscopy results showed that SIINFEKL mainly existed in the vesicles of BMDCs after 12 h treatment with OVAp, Op-SG, and Op-TG, consistent with the route preceding antigen presentation at the cell surface, and more SIINFEKL aggregated in the Op-TG group than in the OVAp and Op-SG group (Fig. 3**B**) Using flow cytometry, we also compared the absorption efficiency of Op-TG in

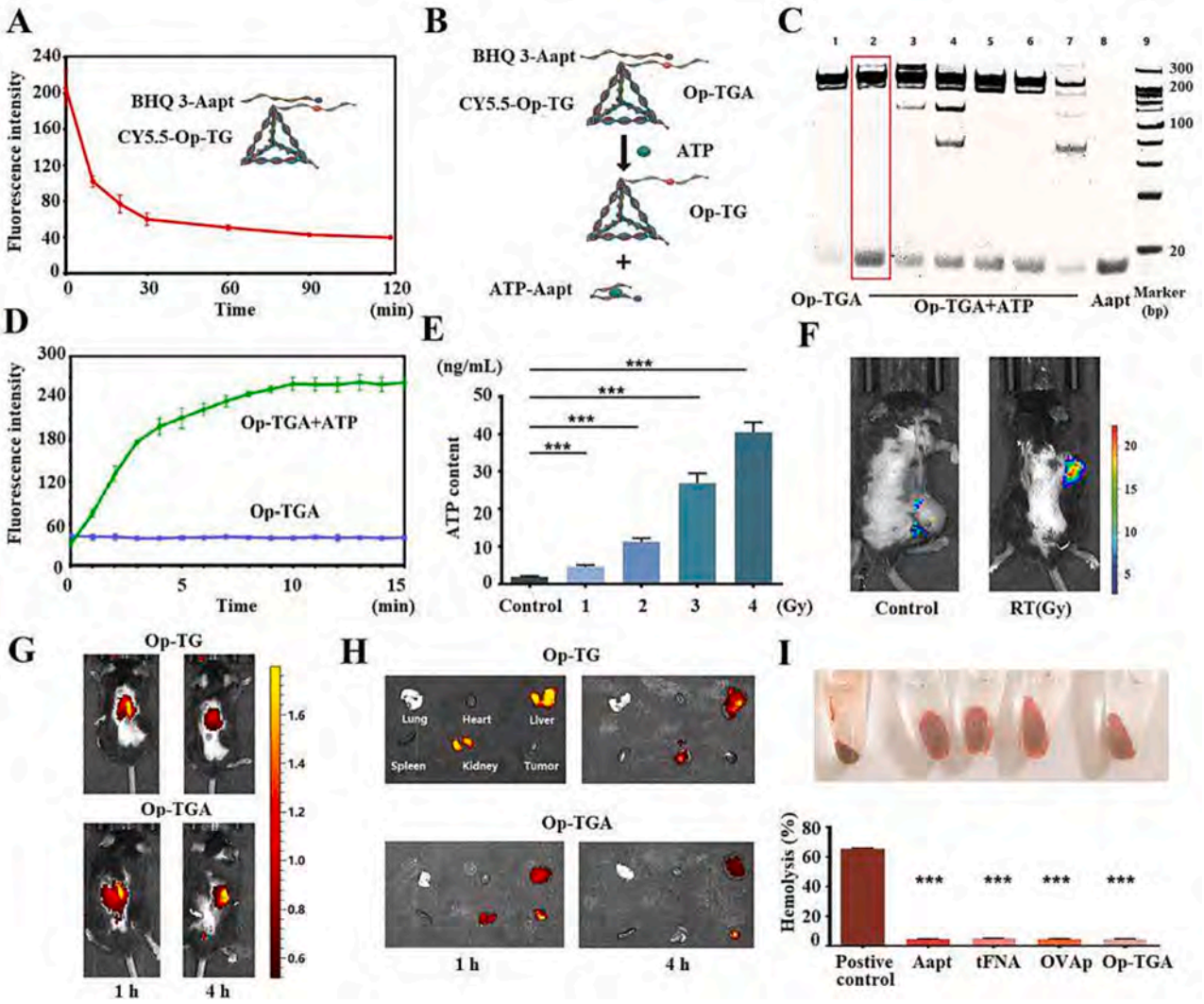

Fig. 2. Controlled release of Op-TGA. (A). Fluorescence intensity of Cy5.5-Op-TG changes with BHQ 3-Aapt. (B). Schematic diagram of ATP-induced de-hybridization of the double strands formed by BHQ 3-modified Aapt and Cy5.5-modified Op-TG. (C). Cumulative Op-TG release from Op-TGA in response to ATP (left to right: Lane 1:Op-TGA; Lane 2: Op-TGA + 10 mM ATP; Lane3: Op-TGA + 100 mM ATP; Lane 4: Op-TGA + 1 M ATP; Lane 5: Op-TGA + 0.5 mM ATP; Lane 6: Op-TGA + 50 mM ATP, Lane 7:Op-TGA + 5 M ATP; Lane 8: Aapt). (D). Changes of CY5.5 fluorescence intensity with time after the addition of 10 mM ATP to Op-TGA, and use the group without ATP as a control. (E). Relationship between radiotherapy dose and ATP concentration released by tumor cells. (F). Observation of ATP concentration in tumor tissue by in vivo imaging in mice (G). The images of the biodistribution in vivo of Op-TG and Op-TGA.(1 μM) (H). In vivo distribution at the organ level. (I). Hemolysis of Op-TGA (1 μM) and its components.

BMDCs and mouse melanoma B16-F10, discovered that Op-TG was difficult to be taken up by B16-F10 cells, demonstrating that it is not necessary to be apprehensive about melanoma consumption while using our delivery platform (**FIG. S6**, **Supporting Information**). After ingesting antigens and immuno-adjuvants, APCs typically reacts in two distinct ways to stimulate a subsequently T-cell-mediated adaptive immune response. Prior to presentation to T cells, antigens attach to major histocompatibility complex I(MHC-I). Moreover, immuno-adjuvants stimulate the maturation of immature DCs [6,33]. The resultant mature DCs express the co-stimulatory molecules CD80 and CD86 on their surface, which, in conjunction with the MHC-I-antigen, boost the T-cell response. Consequently, we examined the impacts of Op-TG on activation and antigen presentation in DCs. By flow cytometry, we established that CD45 + CD11c + BMDCs treated with Op-TGA enhanced the percentage of CD45 + CD11c + BMDCs co-expressing CD80 + and CD86+, and the proportion was significantly higher than that in the pure OVAp group and the Op-SG group. (Fig. 3**C**). By quantifying the production of pro-inflammatory cytokines into the culture media, the immunological response triggered by DC maturation was investigated further. After 24 h of treatment, the secretion of IL-12p70, IL-1β, and TNF-α was considerably higher in the Op-TG group than in other groups (Fig. 3**D**).

Subsequently, we determined the effectiveness of OVAp (SIINFEKL) presentation by BMDCs in the Op-SG group and Op-TG group. the flow cytometry data demonstrated that the proportion of MHC-I-SIINFEKL+ (H-2 kb) in CD45 + CD11c + BMDCs was considerably greater in the Op-TG group than in the Op-SG group (Fig. 3**E**). Similarly, using CLSM to study BMDCs treated with Op-SG and Op-TG for 36 h, the results revealed that more SIINFEKL aggregated on the cell membrane surface and that the antigen presentation efficiency of the Op-TG group was considerably greater than that of the Op-SG group (Fig. 3**F**).

Dendritic cell maturation promotes T-cell-mediated adaptive immunological response. Therefore, we first confirmed that Op-TG-activated BMDCs can stimulate lymphocyte proliferation. When the initial ratio of BMDCs to lymphocytes was greater, the potential of BMDCs to induce lymphocyte proliferation was enhanced. The capacity of Op-TG-activated BMDC to stimulate lymphocyte proliferation was much greater than that of other groups (Fig. 3**G**). Based on the above

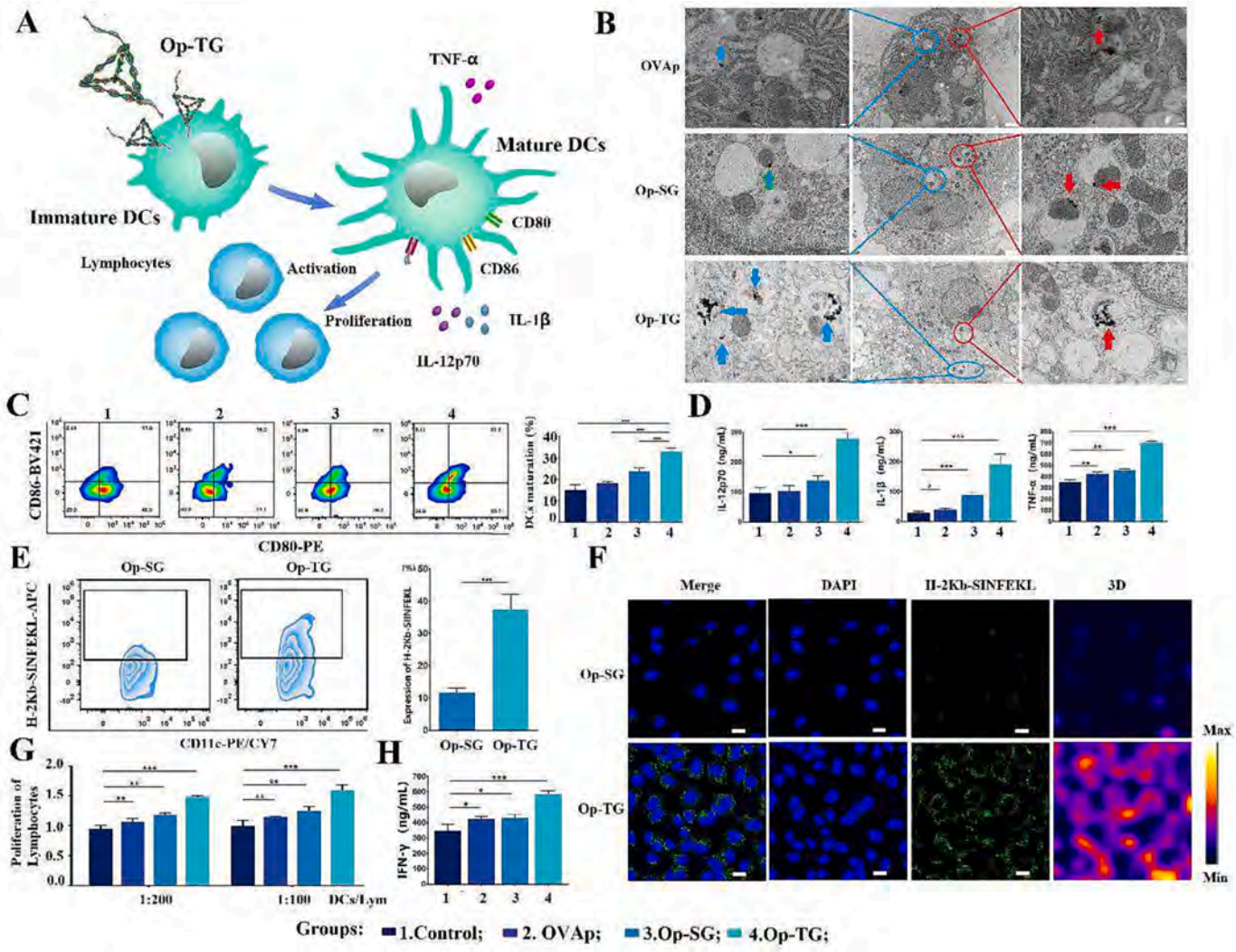

Fig. 3. Op-TG enhances immune responses in vitro. (250 nM) (A). Schematic diagram of Op-TG enhancing immune response. (B). Op-TG aggregation in DCs by TEM, bar: 1 μm, 500 nm. (C). Representative flow cytometry results showing the DCs maturation under different treatments and flow cytometry analyses of CD45 + CD11c + CD80 + CD86 + DCs. (D). IL-12p70, IL-1β, and TNF-α levels secreted by DCs measured after different treatments. (E). Representative flow cytometry results for the efficiency of DC antigen presentation and flow cytometry analysis of antigens presented by DCs (CD45 + CD11C + H-2 Kb +). (F). Immunofluorescence analysis of antigens presented by DCs, bar: 20 μm. (G). DCs stimulate lymphocyte proliferation. (H). IFN-γ levels secreted by DCs in different treatment groups stimulated splenic lymphocytes.

results, the role of DCs in the Op-TG-treated group in inducing specific immune responses was further verified, and we determined the stimulation of IFN-γ secretion by splenic lymphocytes by DCs after treatment with different treatments (DCs/Lym:1:100). The results showed (Fig. 3**H**) that DCs in the Op-TG-treated group were able to stimulate splenic lymphocytes to secrete higher levels of IFN-γ. In conclusion, Op-TG promoted DCs maturation and antigen presentation efficiently. It obviously stimulates the innate and adaptive immune systems and is superior to the pure OVAp and Op-SG groups, confirming the efficacy and superiority of tFNA as a carrier of immuno-adjuvants and antigens.

3.4. Synergistic therapy by using RT and TGA

Next, we assessed the potential of ATP-responsive and immunoadjuvant-functionalized framework nucleic acids (TGA) to improve the therapeutic efficacy of RT in the treatment of mouse tumors. The treatment strategy is shown in Fig. 4**A**. We implanted B16-F10 melanoma tumors on the backs of C57BL/6 mice and began therapy 7 days later. Randomly assigning C57BL/6 mice wit1 B16 melanoma into 6 groups (n > 6): Group 1, Saline; Group 2, RT; Group 3, Aapt-SG (SGA); Group 4, TGA; Group 5, RT + SGA; Group6, RT + TGA. For Groups 3 and 5, SGA refers to the process of incubating Aapt with SG to produce a single-chain structure capable of responding to ATP. In the experiment, 100 μL of 2 μM TGA and SGA was injected into the tail vein of each mouse. On the 1st, 4th, 7th, and 10th day, tumors in Group 2, Group 4, and Group 5 were irradiated locally with a dosage of 3 Gy per mouse. Group 5 and Group 6 were injected SGA and TGA after 16 h of each RT. The tumor growth curve and tumor volumes indicated that TGA and RT alone inhibited tumor development to a limited degree. As anticipated, the combination of RT and TGA exhibited the most effective inhibition of tumors, with an 88.1 % inhibition rate (Fig. 4**B, 4C, and 4D**). Similarly, the tumor weight in the various therapy groups revealed similar patterns (Fig. 4**E**). The photographs, H&E and TUNEL staining of the removed tumors further demonstrated the greater efficacy of the combination of RT and TGA (Fig. 4**F, 4G**). CD31 is a marker of vascular endothelial differentiation and is used to evaluate tumor angiogenesis and determine whether the tumor is growing rapidly. The results demonstrated that Group 6 had considerably less CD31 than the other groups, indicating that tumor development was greatly inhibited in this group (Fig. 4**H**).

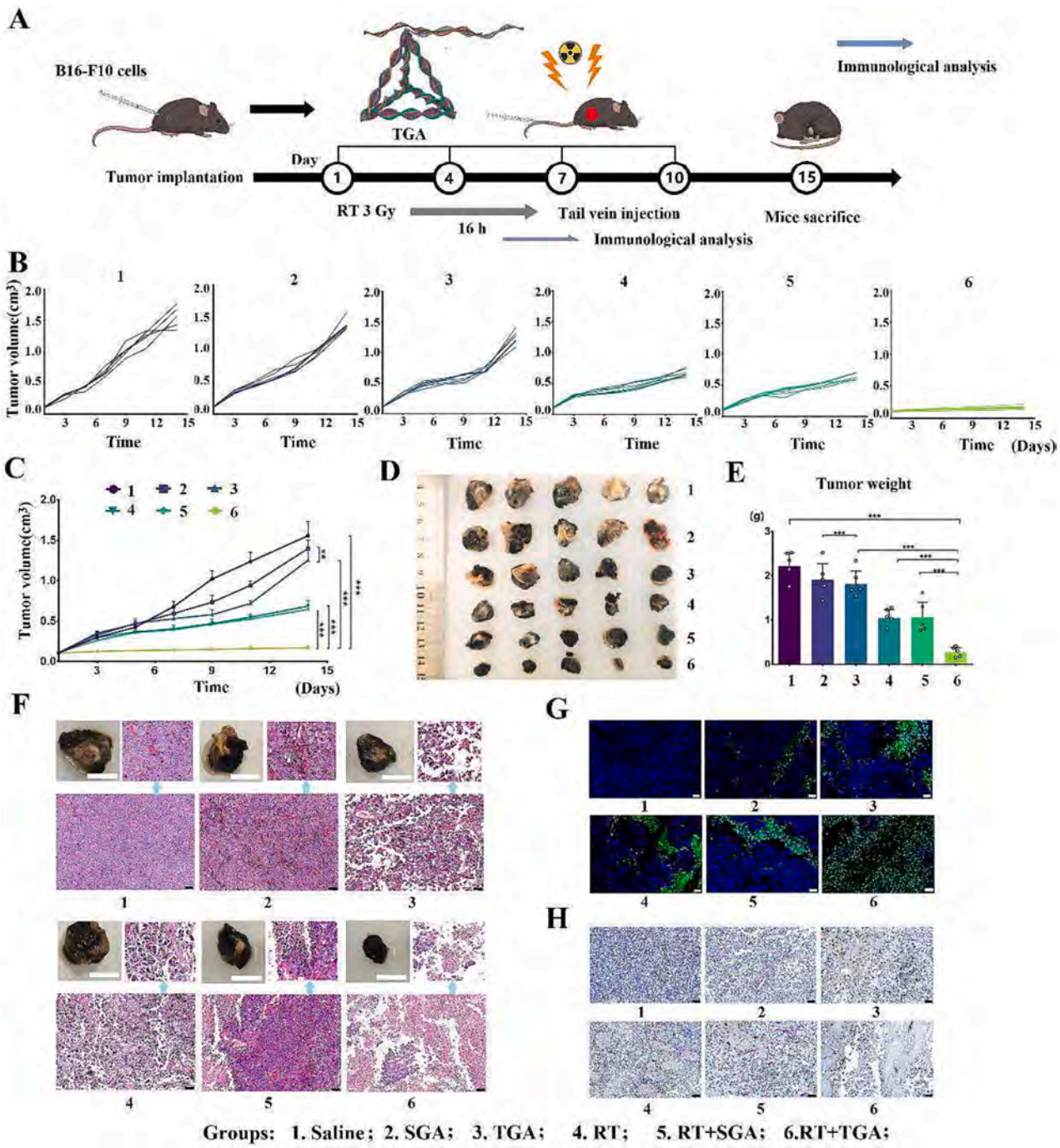

Fig. 4. ATP-Responsive and immunoadjuvant-functionalized framework nucleic acids assisted with Radiotherapy for the treatment of B16-F10 tumor cells. (A). Schematic illustration of the experiment design. (B). Individual tumor growth curves of B16-F10 tumors on mice from different groups as indicated (1 μM). (C). Statistical tumor growth curves. The error bars represent mean ± SEM (n = 6). (D). Tumor photos of different groups, (E). Tumor weight in different treatment groups. (F). H&E staining (bar: 50 μm), and (G). TUNEL staining (bar: 50 μm) of different treatment groups. (H). IHC staining in tumor tissues for CD31 (Red) of different treatment groups, bar: 50 μm. (For interpretation of the references to colour in this figure legend, the reader is referred to the web version of this article.)

3.5. The immune activation effect of TGA in the immune microenvironment

In order to further study the synergistic mechanism of immunoadjuvant-functionalized tetrahedral framework nucleic acid and RT, flow cytometry analysis and multiplex immunofluorescence analysis was performed. Following the treatment strategy mentioned above, we sacrificed the mice in each group on the 7th day to examine changes in immune cell populations in great detail. As shown in Fig. 5**A**, compared to RT alone, the combination of RT and TGA considerably enhanced the maturation of DCs in the inguinal lymph nodes. Furthermore, the efficacy of the TGA was much greater than that of SGA, showing the efficacy of tFNA as an adjuvant delivery vehicle. Simultaneously, we observed co-expression levels of CD11C, CD80, and CD86 in lymph node sections, as well as a significant number of mature DCs in the lymph nodes after RT + TGA therapy (Fig. 5**B**). Regulatory T cells (Treg cells) that promote tumor immune evasion also exist in the TME. In comparison to the other treatment groups, the RT + TGA group had significantly fewer Treg cells in the TME, indicating that the combination of RT and TGA alleviated some of the immunosuppressive effects

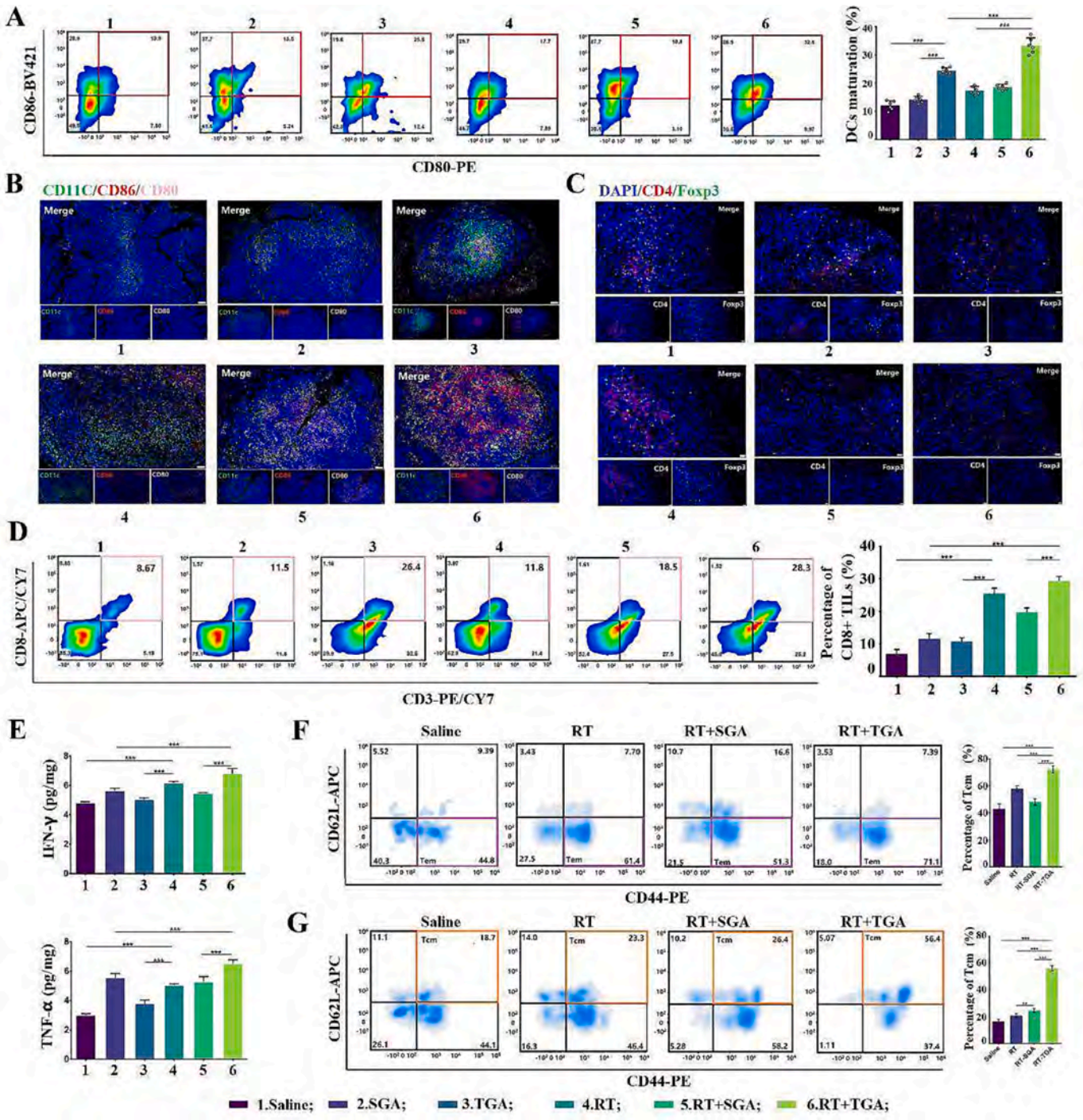

Fig. 5. Op-TGA (1 μM) for synergistic Radiotherapy-immunotherapy induced an immune-active TME. (A). Representative flow cytometry results showing the DCs maturation in lymph nodes under different treatments. (B). Flow cytometry analyses of CD45 + CD11c + CD80 + CD86 + matured DCs in lymph nodes. (C). Immunofluorescence analysis of DC maturation in lymph nodes (bar: 50 μm). (D). Immunofluorescence staining in tumor tissues for Treg cells (Merge), bar: 20 μm. (E). Representative flow cytometry results showing the CD3 + CD8 + T cells in the tumor tissue and flow cytometry analyses of CD3 + CD8 + T cells in the tumor tissue. (F). IFN-γ levels and TNF-α levels in Tumors were measured 7 days later after different treatments. (G). Representative flow cytometry results show the Tem in peripheral blood and flow cytometry analyses of CD3 + CD8 + CD44 + CD62L- Tem. (H). Representative flow cytometry results show Tcm in spleen under different treatments and flow cytometry analyses of CD3 + CD8 + CD44 + CD62L + Tcm.

(Fig. 5**C**). Then, the number of tumor-infiltrating lymphocytes (TILs) in various groups were analyzed, and the results revealed that the proportion of CD3 + CD8 + TILs in the RT + TGA group was dramatically enhanced, approximately 2.8 times greater than that in the Saline group, indicating that the tumor was in an active immune state (Fig. 5**D**). Additionally, we respectively measured levels of TNF-α and IFN-γ, two factors of cellular immunity, in the tumor. Both cytokines were abundantly secreted in serum and tumors after RT + TGA therapy (Fig. 5**E**). Next, we investigated the role of ATP-responsive and immunoadjuvant-functionalized framework nucleic acids in inducing immune memory. Effector memory T cells (Tem) and central memory T cells (Tcm) are the two main subtypes of memory T cells. Tcm predominates in secondary lymphoid tissue, whereas Tem is primarily found in peripheral blood. Thus, 7 days after therapy, we took peripheral

blood and lymph nodes from mice to assess CD8 + T cells. According to the results, mice in the RT + TGA group had a considerably larger percentage of CD8 + Tem in their peripheral blood than mice in the other groups. Similar results were seen with CD8 + Tcm in mouse lymph nodes (Fig. 5**F, 5G**). Abundant memory T cells demonstrate that the RT and TGA combination therapy retains long-lasting anticancer effects.

3.6. Anti-Tumor effects in a tumor model that specifically expresses antigens

The anti-tumor effects of TGA-carrying tumor antigen (OVA peptide) in radio-immunotherapy were then investigated. In this portion of the experiment, OVA-expressing B16-F10 cells (OVA-B16-F10) were injected into the backs of C57BL/6 mice to create melanoma-bearing mice. TGA-carrying OVA peptide (Op-TGA) was injected into tumor-bearing mice via the tail vein, and the antitumor and immunomodulatory effects of Op-TGA and RT were detected (Fig. 6**A**). The combined treatment of RT and Op-TGA in tumor-bearing mice almost inhibited tumor growth with a tumor inhibition rate of 93.9 %, and other treatments were less effective (Fig. 6**B, 6C**). RT + Op-TGA group also greatly prolonged the survival of tumor-bearing mice (Fig. 6**D**). Tumor sections stained with TUNEL demonstrated the same trend in the RT + Op-TGA group. Noting that the therapeutic efficacy of OVA peptide mixed with TGA is not as optimal as that of TGA-carrying OVA peptide, we suggest that when TGA is chemically linked to OVAp, DCs can promptly and abundantly uptake OVAp, enabling DCs to absorb sufficient antigen to trigger a robust immune response. It demonstrates the efficacy of tFNA as an antigen transporter. Simultaneously, we performed H&E staining on sections of the mice's major organs. The result revealed that there were no visible pathological changes in the organs of mice treated with RT + Op-TGA, indicating that the substance had minor negative effects (**FIG. S7, Supporting Information**).

3.7. Op-TGA activates the cellular immune response and promotes immune memory effects

Subsequently, immunological analysis was conducted on each therapy group. Similarly studied were the dendritic cells in the lymph nodes, where the proportion of CD11c + CD80 + CD86 + cells was also significantly elevated (Fig. 6**G**). Then, we analyzed T cells in the spleen using flow cytometry and immunofluorescence because the spleen is an important immune organ and the main site for immune cell homing and differentiation. The results showed that after RT and Op-TGA combined treatment, T lymphocytes, particularly CD8 + T cells, were significantly increased in the spleen of mice (FIG.. 6 h). Op-TGA generated a substantial number of T lymphocytes, primarily CD3 + CD8 + T cells, to infiltrate the tumor (Fig. 6**I, 6 J, and 6 K**). As depicted in Fig. 5i, CD8 + cells multiply at the tumor tissue margin, indicating that a significant number of cytotoxic T lymphocytes exerted antitumor effects. Tem cells in the peripheral blood (Fig. 6**L**) and Tcm cells in the spleen (Fig. 6**M**) confirmed that the combination of RT and Op-TGA can elicit superior immunological memory effects. In addition, the mice of the RT + Op-TGA group were re-implanted with OVA-B16-F10 on the opposite side of their backs on 15th, while naive mice were utilized as controls. After 20 days, no tumor development was seen in mice treated with RT + Op-TGA. It provides more proof that the combination of RT and Op-TGA can induce excellent immunological memory effects to prevent tumor recurrence (Fig. 6**N**).

4. Discussion and conclusions

Although RT is still one of the current mainstream treatment techniques for solid tumors, its efficacy is limited for some cancers with high aggressiveness and recurrence rate, such as melanoma [34]. Because melanoma is inherently resistant to traditional radiation, metastatic melanoma patients have a terrible prognosis, with a less than 10 % 3-year survival rate [34,35]. Despite the fact that numerous radiosensitizers and systemically administered immune stimulants have been developed in recent studies for radiotherapy-resistant tumors, these treatment strategies can result in severe side effects, such as systemic cytokine storm, multiple local injections causing adverse reactions, etc. [36]. In addition, the majority of clinical applications involve low-dose radiation therapy to prevent damage to normal tissue surrounding the tumor, although it is challenging to get the optimal therapeutic efficacy [37]. Therefore, the utilization of nanotechnology to produce TME-targeted immune adjuvants and specialized antigen delivery platforms can most effectively compensate for the limitations of radiation [38,39]. Furthermore, the development of nano-delivery systems that can respond to high ATP levels and release substances that can activate local adaptive immunity in tumors is an excellent method for enhancing the efficacy of RT.

The data indicate that RT alone inhibits melanoma tumor growth in mice by only approximately 15 %, which is extremely disappointing (Figs. 4, 6). In addition, the effects of RT on adaptive immune response and immunological memory are minimal (Figs. 5, 6). To enhance the therapeutic efficacy, an ATP-responsive and immunoadjuvant-functionalized framework nucleic acid delivery system was developed that not only accumulated massively surrounding irradiated tumor tissue, but also released tFNAs carrying antigenic peptides and immune adjuvants at high ATP concentrations. The results show that this delivery system can enter DCs, increase DCs maturation, effectively present antigens, and stimulate the proliferation of T lymphocytes. In vivo, the combination of RT and Op-TGA inhibited tumor growth by 93.9 % and decreased mice mortality during treatment. We validated the effect of tFNA on immunoadjuvant functionalization and delivery of antigens in two B16 melanoma mouse models that did not express OVA and that did express OVA, demonstrating that it has the following benefits: (1) promoting DCs maturation through co-stimulatory signals (CD80/86 and cytokine IL-12p70) that mediate cytotoxic T cell activation, (2) promoting massive T cell infiltration into tumors, (3) diminish immunosuppressive effects in the TME, and (4) elicit potent immunological memory effects.

DCs are central to the initiation of cellular immune responses [42]. Therefore, we analyzed the maturation of DCs in TDLNs in the early stages of treatment. Flow cytometry analysis showed that the addition of TGA at the time of radiotherapy further increased the proportion of mature DCs, suggesting that TGA-loaded CpG can be transported into the interior of DCs to undergo immunostimulatory effects. In the anti-tumor immune response, mature DCs can activate specific immune responses mediated by T lymphocytes. Therefore, we speculated that TGA could cause a stronger anti-tumor immune response compared to radiotherapy. The immunotherapeutic effects of TGA in combination with radiotherapy were analyzed by flow cytometry, multiplex immunofluorescence, and ELISA. The experimental results showed that the proportion of CTLs in TILs significantly increased in the RT + TGA treatment group, the secretion of tumor-associated cytokines IFN-γ and TNF-α was increased, and the Tregs with immuno-suppressive effects around the tumor tissues were significantly reduced. All these phenomena demonstrated that when TGA was used in combination with radiotherapy, it was by increasing the proportion of mature DCs, which activated a more intense downstream immune response and further expanded the RT-induced anti-tumor immune response.

Typically, nano-delivery techniques have possible safety risks [38–41]. For instance, whether intravenous infusion induces hemolysis or if there is organ toxicity. We investigated the hemolysis coefficient of each component of Op-TGA; none of the components caused hemolysis, and H&E staining of major organs revealed that the delivery system caused minimal harm to normal organs.

The unique feature of our created delivery system is that it can synergize with radiotherapy to compensate for the side effects of low-dose radiotherapy, and its simple injection method and environmental targeting considerably improve this strategy's applicability. And

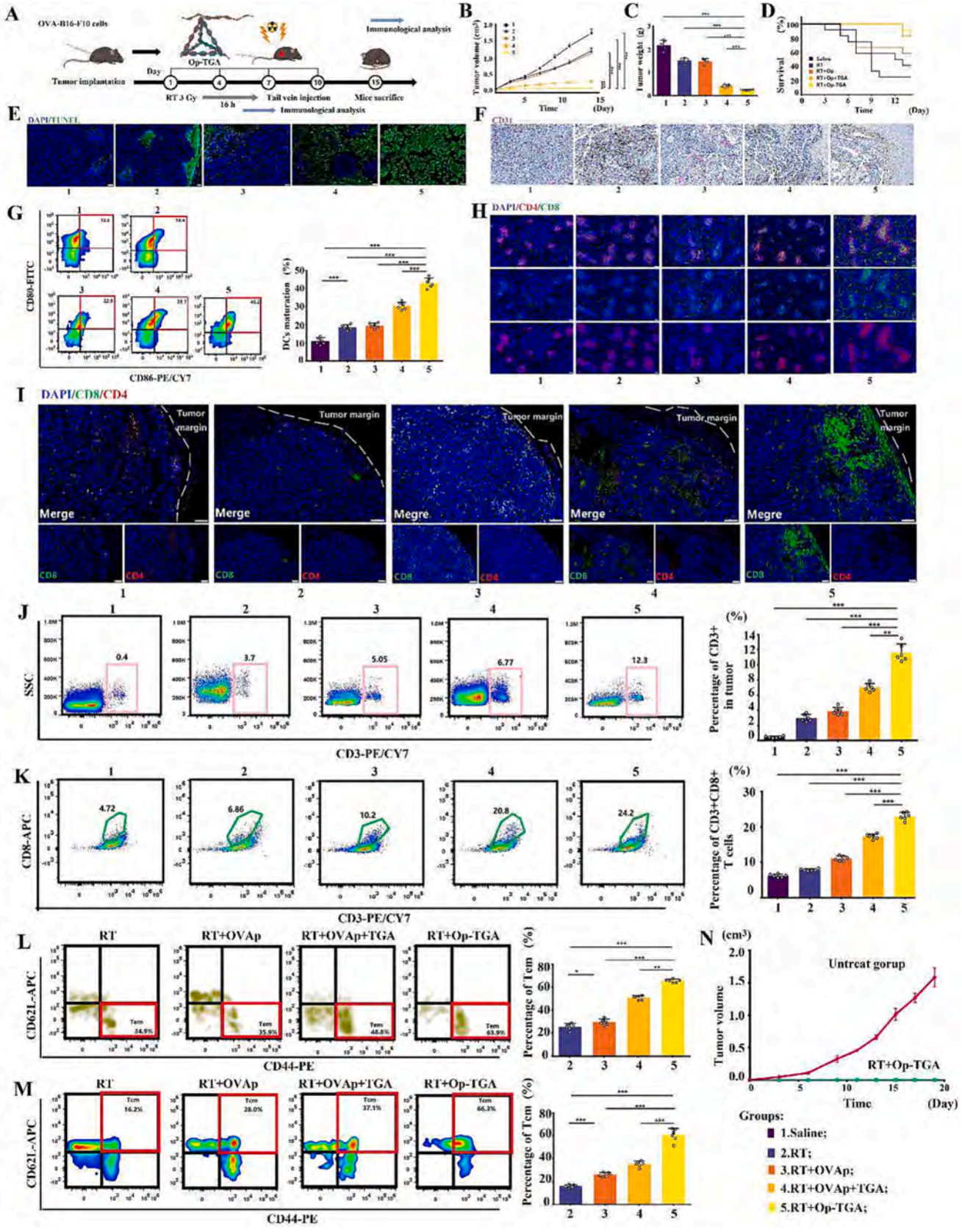

(caption on next page)

Fig. 6. ATP-Responsive and functionalized framework nucleic acids assisted with Radiotherapy for the treatment of OVA-B16-F10 melanoma and immunological analysis. (A). Schematic illustration of the experiment design. (B). Statistical tumor growth curves. The error bars represent mean ± SEM (n = 6). (C). Tumor weight in different treatment groups. (D). Survival rates of OVA-B16 tumor-bearing mice post different treatments as indicated. (E). TUNEL staining of different treatment groups, bar: 50 μm. (F). IHC staining in tumor tissues for CD31 (Red) of different treatment groups. bar: 50 μm. (G). Representative flow cytometry results and analyses of CD45 + CD11c + CD80 + CD86 + matured DCs in lymph nodes. (H). The typing of T cells in the spleen was observed by immunofluorescence. (I). Fluorescence images of CD8 + T cells and CD4 + T cells in a tumor and in tumour marginal tissue. (J). Representative flow cytometry results and analyses of CD3 + T cells in the tumor tissue, bar: 100 μm. (K). Representative flow cytometry results and analyses of CD3 + CD8 + T cells in the tumor tissue. (L). Representative flow cytometry results and flow cytometry analyses of CD3 + CD8 + CD44 + CD62L- Tem in peripheral blood. (M). Representative flow cytometry results and flow cytometry analyses of CD3 + CD8 + CD44 + CD62L + Tcm in the spleen. (N). Re-challenged tumor growth curves for the untreated and RT + Op-TGA groups. The error bars reflect the mean standard deviation (n = 6). (For interpretation of the references to colour in this figure legend, the reader is referred to the web version of this article.)

because the delivery system has a high level of biosafety, it has a strong potential for clinical translation.

Declaration of Competing Interest

The authors declare that they have no known competing financial interests or personal relationships that could have appeared to influence the work reported in this paper.

Data availability

Data will be made available on request.

Acknowledgments

This study was funded by the National Key R&D Program of China (2019YFA0110600) and National Natural Science Foundation of China (Grant Nos. 82370929, 81970916, 81671031, and 81901059), Sichuan Science and Technology Program (2022NSFSC0002), Sichuan Province Youth Science and Technology Innovation Team (2022JDTD0021), Research and Develop Program, West China Hospital of Stomatology Sichuan University (RD03202302).We would like to thank Dr. Chenghui Li, Analytical and Testing Center, Sichuan University, for assisting with capturing laser scanning confocal images.

Appendix A. Supplementary data

Supplementary data to this article can be found online at https://doi.org/10.1016/j.cej.2023.146278.

References

[1] G. Kroemer, L. Galluzzi, O. Kepp, L. Zitvogel, Immunogenic cell death in cancer therapy, Annu. Rev. Immunol. 31 (2013) 51–72, https://doi.org/10.1146/annurev-immunol-032712-100008.
[2] D.R. Green, T. Ferguson, L. Zitvogel, G. Kroemer, Immunogenic and tolerogenic cell death, Nat. Rev. Immunol. 9 (5) (2009) 353–363, https://doi.org/10.1038/nri2545.
[3] I. Martins, Y. Wang, M. Michaud, Y. Ma, A.Q. Sukkurwala, S. Shen, O. Kepp, D. Métivier, L. Galluzzi, J.L. Perfettini, L. Zitvogel, G. Kroemer, Molecular mechanisms of ATP secretion during immunogenic cell death, Cell Death Differ. 21 (1) (2014) 79–91, https://doi.org/10.1038/cdd.2013.75.
[4] P. Sharma, J.P. Allison, The future of immune checkpoint therapy, Science (New York, N.Y.) 348(6230) (2015) 56-61. https://doi.org/10.1126/science.aaa8172.
[5] S.K. Wculek, F.J. Cueto, A.M. Mujal, I. Melero, M.F. Krummel, Dendritic cells in cancer immunology and immunotherapy, Nat. Rev. Immunol. 20 (1) (2020) 7–24, https://doi.org/10.1038/s41577-019-0210-z.
[6] H. Tanaka, H. Matsushima, A. Nishibu, B.E. Clausen, A. Takashima, Dual therapeutic efficacy of vinblastine as a unique chemotherapeutic agent capable of inducing dendritic cell maturation, Cancer Res. 69 (17) (2009) 6987–6994, https://doi.org/10.1158/0008-5472.can-09-1106.
[7] C. Vanpouille-Box, S.C. Formenti, S. Demaria, Toward Precision Radiotherapy for Use with Immune Checkpoint Blockers, Clinical cancer research : an official journal of the American Association for, Cancer Res. 24 (2) (2018) 259–265, https://doi.org/10.1158/1078-0432.ccr-16-0037.
[8] M.V. Maus, J.A. Fraietta, B.L. Levine, M. Kalos, Y. Zhao, C.H. June, Adoptive immunotherapy for cancer or viruses, Annu. Rev. Immunol. 32 (2014) 189–225, https://doi.org/10.1146/annurev-immunol-032713-120136.
[9] J. Scheiermann, D.M. Klinman, Clinical evaluation of CpG oligonucleotides as adjuvants for vaccines targeting infectious diseases and cancer, Vaccine 32 (48) (2014) 6377–6389, https://doi.org/10.1016/j.vaccine.2014.06.065.
[10] J. Pan, Y. Wang, C. Zhang, X. Wang, H. Wang, J. Wang, Y. Yuan, X. Wang, X. Zhang, C. Yu, S.K. Sun, Antigen-Directed Fabrication of a Multifunctional Nanovaccine with Ultrahigh Antigen Loading Efficiency for Tumor Photothermal-Immunotherapy, Adv. Mater. 30 (8) (2018), https://doi.org/10.1002/adma.201704408.
[11] J. Wu, J. Chen, An immune cocktail therapy to realize multiple boosting of the cancer-immunity cycle by combination of drug/gene delivery nanoparticles, Sci. Adv. 6 (40) (2020), https://doi.org/10.1126/sciadv.abc7828.
[12] F. Steinhagen, T. Kinjo, C. Bode, D.M. Klinman, TLR-based immune adjuvants, Vaccine 29 (17) (2011) 3341–3355, https://doi.org/10.1016/j.vaccine.2010.08.002.
[13] L. Wu, W. Zhou, L. Lin, A. Chen, J. Feng, X. Qu, H. Zhang, J. Yue, Delivery of therapeutic oligonucleotides in nanoscale, Bioact. Mater. 7 (2022) 292–323, https://doi.org/10.1016/j.bioactmat.2021.05.038.
[14] M. Ovais, S. Mukherjee, A. Pramanik, D. Das, A. Mukherjee, A. Raza, C. Chen, Designing Stimuli-Responsive Upconversion Nanoparticles that Exploit the Tumor Microenvironment, Adv. Mater. 32 (22) (2020) e2000055.
[15] K. Cheng, R. Zhao, Y. Li, Y. Qi, Y. Wang, Y. Zhang, Bioengineered bacteria-derived outer membrane vesicles as a versatile antigen display platform for tumor vaccination via Plug-and-Display technology, Nat. Biomed. Eng. 12 (1) (2021) 2041, https://doi.org/10.1038/s41467-021-22308-8.
[16] J. Wu, J. Chen, Y. Feng, H. Tian, X. Chen, Tumor microenvironment as the "regulator" and "target" for gene therapy, J. Gene Med. 21 (7) (2019) e3088.
[17] W. Ma, Y. Yang, J. Zhu, W. Jia, T. Zhang, Z. Liu, X. Chen, Y. Lin, Biomimetic Nanoerythrosome-Coated Aptamer-DNA Tetrahedron/Maytansine Conjugates: pH-Responsive and Targeted Cytotoxicity for HER2-Positive Breast Cancer, Adv. Mater. (2022) e2109609.
[18] J. Zhu, Y. Yang, W. Ma, Y. Wang, L. Chen, H. Xiong, C. Yin, Z. He, W. Fu, R. Xu, Y. Lin, Antiepilepticus Effects of Tetrahedral Framework Nucleic Acid via Inhibition of Gliosis-Induced Downregulation of Glutamine Synthetase and Increased AMPAR Internalization in the Postsynaptic Membrane, Nano Lett. 22 (6) (2022) 2381–2390, https://doi.org/10.1021/acs.nanolett.2c00025.
[19] M. Zhang, X. Zhang, T. Tian, Q. Zhang, Y. Wen, J. Zhu, D. Xiao, W. Cui, Y. Lin, Anti-inflammatory activity of curcumin-loaded tetrahedral framework nucleic acids on acute gouty arthritis, Bioact. Mater. 8 (2022) 368–380, https://doi.org/10.1016/j.bioactmat.2021.06.003.
[20] T. Zhang, T. Tian, R. Zhou, S. Li, W. Ma, Y. Zhang, N. Liu, S. Shi, Q. Li, X. Xie, Y. Ge, M. Liu, Q. Zhang, S. Lin, X. Cai, Design, fabrication and applications of tetrahedral DNA nanostructure-based multifunctional complexes in drug delivery and biomedical treatment, Nature Protocol 15 (8) (2020) 2728–2757, https://doi.org/10.1038/s41596-020-0355-z.
[21] M. Zhou, T. Zhang, B. Zhang, X. Zhang, S. Gao, T. Zhang, S. Li, X. Cai, A DNA Nanostructure-Based Neuroprotectant against Neuronal Apoptosis via Inhibiting Toll-like Receptor 2 Signaling Pathway in Acute Ischemic Stroke, ACS Nano (2021), https://doi.org/10.1021/acsnano.1c09626.
[22] J. Li, Y. Lai, M. Li, X. Chen, M. Zhou, W. Wang, J. Li, W. Cui, G. Zhang, K. Wang, L. Liu, Y. Lin, Repair of infected bone defect with Clindamycin-Tetrahedral DNA nanostructure Complex-loaded 3D bioprinted hybrid scaffold, Chem. Eng. J. 435 (2022), 134855, https://doi.org/10.1016/j.cej.2022.134855.
[23] Y. Li, S. Gao, S. Shi, D. Xiao, S. Peng, Y. Gao, Y. Zhu, Y. Lin, Tetrahedral Framework Nucleic Acid-Based Delivery of Resveratrol Alleviates Insulin Resistance: From Innate to Adaptive Immunity, Nano-Micro Letters 13 (1) (2021) 86, https://doi.org/10.1007/s40820-021-00614-6.
[24] Y. Wang, Y. Li, S. Gao, X. Yu, Y. Chen, Y. Lin, Tetrahedral Framework Nucleic Acids Can Alleviate Taurocholate-Induced Severe Acute Pancreatitis and Its Subsequent Multiorgan Injury in Mice, Nano Lett. 22 (4) (2022) 1759–1768, https://doi.org/10.1021/acs.nanolett.1c05003.
[25] X. Qin, L. Xiao, N. Li, C. Hou, W. Li, J. Li, N. Yan, Y. Lin, Tetrahedral framework nucleic acids-based delivery of microRNA-155 inhibits choroidal neovascularization by regulating the polarization of macrophages, Bioact. Mater. 14 (2022) 134–144, https://doi.org/10.1016/j.bioactmat.2021.11.031.
[26] J. Li, Y. Yao, Y. Wang, J. Xu, D. Zhao, M. Liu, S. Shi, Modulation of the Crosstalk between Schwann Cells and Macrophages for Nerve Regeneration: A Therapeutic Strategy Based on a Multifunctional Tetrahedral Framework Nucleic Acids System, Advanced Materials (2022) e2202513. https://doi.org/10.1002/adma.202202513.
[27] B. Zhang, T. Tian, D. Xiao, S. Gao, X. Cai, Y. Lin, Facilitating In Situ Tumor Imaging with a Tetrahedral DNA Framework-Enhanced Hybridization Chain Reaction Probe, Adv. Funct. Mater. 32 (16) (2022) 2109728, https://doi.org/10.1002/adfm.202109728.
[28] M. Liu, W. Ma, D. Zhao, J. Li, Q. Li, Y. Liu, Enhanced Penetrability of a Tetrahedral Framework Nucleic Acid by Modification with iRGD for DOX-Targeted Delivery to

Triple-Negative Breast Cancer, ACS Appl. Mater. Interfaces 13 (22) (2021) 25825–25835, https://doi.org/10.1021/acsami.1c07297.
[29] Y. Zhang, C. Mao, Y. Zhan, Y. Zhao, Y. Chen, Y. Lin, Albumin-Coated Framework Nucleic Acids as Bionic Delivery System for Triple-Negative Breast Cancer Therapy, ACS Appl. Mater. Interfaces 14 (35) (2022) 39819–39829, https://doi.org/10.1021/acsami.2c10612.
[30] Y.M.D. Gnopo, H.C. Watkins, T.C. Stevenson, M.P. DeLisa, D. Putnam, Designer outer membrane vesicles as immunomodulatory systems - Reprogramming bacteria for vaccine delivery, Adv. Drug Deliv. Rev. 114 (2017) 132–142, https://doi.org/10.1016/j.addr.2017.05.003.
[31] T. Zhang, M. Zhou, D. Xiao, Z. Liu, Y. Jiang, M. Feng, Y. Lin, X. Cai, Myelosuppression Alleviation and Hematopoietic Regeneration by Tetrahedral-Framework Nucleic-Acid Nanostructures Functionalized with Osteogenic Growth Peptide, Adv. Mater. (2022) e2202058.
[32] L. Sun, F. Shen, L. Tian, H. Tao, Z. Xiong, J. Xu, Z. Liu, ATP-Responsive Smart Hydrogel Releasing Immune Adjuvant Synchronized with Repeated Chemotherapy or Radiotherapy to Boost Antitumor Immunity, Adv. Mater. 33 (18) (2021) e2007910.
[33] L. Ma, T. Dichwalkar, Enhanced CAR-T cell activity against solid tumors by vaccine boosting through the chimeric receptor, Science (New York, N.Y.) 365(6449) (2019) 162-168. https://doi.org/10.1126/science.aav8692.
[34] H. Ledford, Melanoma drug wins US approval, Nature 471 (7340) (2011) 561, https://doi.org/10.1038/471561a.
[35] P.A. Ott, Z. Hu, D.B. Keskin, S.A. Shukla, J. Sun, D.J. Bozym, W. Zhang, A. Luoma, A. Giobbie-Hurder, L. Peter, C. Chen, O. Olive, T.A. Carter, S. Li, D.J. Lieb, T. Eisenhaure, E. Gjini, J. Stevens, W.J. Lane, I. Javeri, K. Nellaiappan, A. M. Salazar, H. Daley, M. Seaman, E.I. Buchbinder, C.H. Yoon, M. Harden, N. Lennon, S. Gabriel, S.J. Rodig, D.H. Barouch, J.C. Aster, G. Getz, K. Wucherpfennig, D. Neuberg, J. Ritz, E.S. Lander, E.F. Fritsch, N. Hacohen, C. J. Wu, An immunogenic personal neoantigen vaccine for patients with melanoma, Nature 547 (7662) (2017) 217–221, https://doi.org/10.1038/nature22991.
[36] Y. Wang, Advances in Hypofractionated Irradiation-Induced Immunosuppression of Tumor Microenvironment, Front. Immunol. 11 (2020), 612072, https://doi.org/10.3389/fimmu.2020.612072.
[37] W. Wang, H. Xu, Q. Ye, F. Tao, I. Wheeldon, Systemic immune responses to irradiated tumours via the transport of antigens to the tumour periphery by injected flagellate bacteria, Nat. Biomed. Eng. 6 (1) (2022) 44–53, https://doi.org/10.1038/s41551-021-00834-6.
[38] J.P.M. Almeida, A.Y. Lin, E.R. Figueroa, A.E. Foster, R.A. Drezek, In vivo gold nanoparticle delivery of peptide vaccine induces anti-tumor immune response in prophylactic and therapeutic tumor models, Small 11 (12) (2015) 1453–1459, https://doi.org/10.1002/smll.201402179.
[39] D. Zamarin, R.B. Holmgaard, S.K. Subudhi, J.S. Park, M. Mansour, P. Palese, T. Merghoub, J.D. Wolchok, J.P. Allison, Localized oncolytic virotherapy overcomes systemic tumor resistance to immune checkpoint blockade immunotherapy, Sci. Transl. Med. 6 (226) (2014) 226ra32, https://doi.org/10.1126/scitranslmed.3008095.
[40] Q. Hu, M. Wu, C. Fang, C. Cheng, M. Zhao, W. Fang, P.K. Chu, Y. Ping, G. Tang, Engineering nanoparticle-coated bacteria as oral DNA vaccines for cancer immunotherapy, Nano Lett. 15 (4) (2015) 2732–2739, https://doi.org/10.1021/acs.nanolett.5b00570.
[41] L. Feng, K. Li, X. Shi, M. Gao, J. Liu, Z. Liu, Smart pH-responsive nanocarriers based on nano-graphene oxide for combined chemo- and photothermal therapy overcoming drug resistance, Adv. Healthc. Mater. 3 (8) (2014) 1261–1271, https://doi.org/10.1002/adhm.201300549.
[42] Q. Tu, Y. Li, J. Zhu, L. Guo, C. Liu, L. Liu, Y. Yuan, Y. Zou, F. Chen, L. Yao, J. Li, Mitochondrial DNA mediates immunoparalysis of dendritic cells in sepsis via STING signalling, Cell Prolif. 55 (12) (2022) e13328.